The Australian National University
Research School of Physical Sciences

ANU-PRL-PP-89/7

DIFFRACTION TOMOGRAPHY FOR PLASMA REFRACTIVE INDEX MEASUREMENTS

John Howard, Raffi Nazikian[1] and Les Sharp
Plasma Research Laboratory
Research School of Physical Sciences
Australian National University
Canberra, A.C.T., AUSTRALIA

Plasma Research Laboratory

ANU-PRL-PP-89/7

DIFFRACTION TOMOGRAPHY FOR PLASMA REFRACTIVE INDEX MEASUREMENTS

John Howard, Raffi Nazikian[1] and Les Sharp
Plasma Research Laboratory
Research School of Physical Sciences
Australian National University
Canberra, A.C.T., AUSTRALIA

Abstract

Measurement of the properties of probing beams of coherent electromagnetic radiation yields essential information about the line of sight integrated plasma refractive index. We present a scalar diffraction treatment of forward angle scattering plasma diagnostics based on the diffraction projection theorem first presented by Wolf[2] . New results are obtained for near field scattering from probing Gaussian beams and it is demonstrated that the effects of diffraction need to be addressed for tomographic inversion of near field scattering and interferometry data.

[1] Princeton Plasma Physics Laboratory, Princeton University, Princeton N.J., U.S.A.

[2] WOLF, E., *The Three Dimensional Structure Determination of Semi-Transparent Objects from Holographic Data*, Opt. Commun., 1, 153 (1969)

1 INTRODUCTION

Line of sight integrated measurements of the plasma refractive index (forward angle scattering, interferometry, shadowgraphy etc.) have provided essential information for the diagnosis and understanding of both the bulk plasma properties [YOUNG *et al.* (1964), HOWARD *et al.* (1967)] and more recently, the nature of both magnetohydrodynamic (MHD) and turbulent density fluctuation phenomena [e.g. JACOBSON (1962), NAZIKIAN and SHARP (1987), KIM *et al.* (1988), WEISEN *et al.* (1988)]. With the development of high spatial resolution diagnostics for density perturbation measurements, it is essential to understand the effects of diffraction from high wavenumber spatial structures upon the detected wave field. In particular, the consequences for interferometry need careful examination.

In this paper we describe a simple linear systems model of the scalar diffraction from refractive index irregularities in a plasma. The model, based on the *diffraction projection theorem* as first revealed by WOLF (1969), embraces all currently employed forward angle, refractivity based diagnostic techniques. The theorem has found extensive application in such diverse fields as acoustic holography, medical imaging and seismic mapping [see KAK (1985) for further information]. It gives a new and intuitive insight into the problem of scattering from plasma fluctuations. General results obtained for plane waves are extended to Gaussian beams, with particular emphasis on the near field properties of the scattered field.

Sections 2 and 3 briefly outline relevant aspects of scalar diffraction theory. The diffraction projection theroem is discussed in Sec. 4. Attention is paid to the conditions under which the result can be validly applied to forward angle plasma scattering experiments with particular emphasis on the Born and Rytov approximations for *weakly-fluctuating* media. We obtain a simple linear transfer function relationship between the k-space properties of the scattered field and the properties of the incident field and scattering medium.

In Sec. 5, properties of the scattered field for the idealized case of plane wave illumination are considered. This leads naturally to an examination of the correspondence between the behaviour of the scattered field and the properties of the scattering medium for certain limiting observational geometries. In this work we concentrate on the *near field* properties of the diffracted field where the phase information, essential for producing an image of the source distribution, is preserved. The usual experimental case of Gaussian beam illumination is then treated in some detail (Sec. 7). Numerical simulations relevant for imaging and multi-channel interferometry are presented in the final part of the paper. It is demonstrated that, in most cases, the effects of diffraction need to be addressed when attempting to tomographically infer density distributions from interferometrically determined plasma phase shift measurements.

2 DIFFRACTION FROM DENSITY FLUCTUATIONS

Scattering of an incident monochromatic wave ($\omega_0 = ck_0$, $k_0 = 2\pi/\lambda_0$) from plasma inhomogeneities of spatial dimension Λ much larger than the plasma Debye length, and of frequency much less than the plasma frequency, (e.g. plasma drift waves or magnetohydrodynamic (MHD) phenomena) is dominated by the collective motions of electrons which follow the macroscopic density variations [SHEFFIELD (1975)]. Provided the scale size of these irregularities is greater than or comparable to the probing wavelength ($\Lambda \gtrsim \lambda_0$) the scattering process can be conveniently handled in terms of the macroscopic diffraction of radiation from an inhomogeneous refractive medium.

We consider the line of sight propagation of an arbitrary incident wave through an inhomogeneous, weakly fluctuating plasma. The electric field at position $P(\mathbf{r})$, $\mathbf{r} = (x, y, z)$ is taken to have the form

$$\mathbf{E}_0(\mathbf{r}, t) = \mathbf{E}_0(\mathbf{r}) \exp(-j\omega_0 t) \tag{2.1}$$

where $\mathbf{E}_0(\mathbf{r})$ is the spatial distribution of the electric field. The propagation of the incident wave in the plasma is determined by the relative permittivity $\overleftrightarrow{\epsilon}_r$, which is a complex tensor quantity

that varies with both position and time. In the following, we assume that the plasma is spatially inhomogeneous, but otherwise lossless (transparent), non-magnetic and varying sufficiently slowly in time that retarded quantities can be evaluated at the observer time (low-temperature approximation) [SHEFFIELD (1975)].

The stated conditions are satisfied for electromagnetic wave propagation in ordinary mode ($\mathbf{E}_0 \| \mathbf{B}_{plasma}$) for which, ignoring the effects of collisions, we may write

$$\overleftrightarrow{\epsilon}_r(\mathbf{r},t) = \epsilon_r(\mathbf{r},t) = 1 - \frac{n_e(\mathbf{r},t)}{n_{cr}}. \tag{2.2}$$

where $n_e(\mathbf{r},t)$ is the electron density, $n_{cr} = k_0^2/(4\pi r_e)$ is the critical density above which the incident electromagnetic wave is reflected and r_e is the classical electron radius. It will be shown below that the plasma can be regarded as weakly fluctuating provided that the normalized electron density [3] $n = n_e/n_{cr}$ is small in a well defined sense.

The wave equation can be expressed in terms of the electric displacement $\mathbf{D} = \epsilon_0 \epsilon_r \mathbf{E}$ as [JACKSON, (1975)]:

$$(\nabla^2 - \frac{1}{c^2}\frac{\partial^2}{\partial t^2})\mathbf{D} = \mathbf{f} \tag{2.3}$$

where

$$\mathbf{f}(\mathbf{r},t) = -\nabla \times \nabla \times [\mathbf{D}(\mathbf{r},t) - \epsilon_0 \mathbf{E}(\mathbf{r},t)] \tag{2.4}$$

is the *scattering potential*. Equation (2.3) is an inhomogeneous Helmholtz equation.

In free space, $\mathbf{f} = 0$, $\mathbf{E} = \mathbf{E}_0$ and Eq. (2.3) reduces to the homogeneous Helmholtz equation

$$(\nabla^2 + k_0^2)\mathbf{E}_0 = 0. \tag{2.5}$$

The general solution of Eq. (2.5) is a linear superposition of plane waves (Sec. 3).

The total field $\mathbf{E}$ at any point in the medium consists of both the free space (incident) and scattered contributions

$$\mathbf{E} = \mathbf{E}_0 + \mathbf{E}_s. \tag{2.6}$$

The solution of the inhomogeneous wave equation for $\mathbf{E}$ is obtained using standard Green's function techniques. Provided $P(\mathbf{r})$ is in the *radiation zone* ($k_0 |\mathbf{r} - \mathbf{r}'| \gg 1$) the scattered component can be expressed as (see e.g. [SURKO and SLUSHER (1980)])

$$\mathbf{E}_s(\mathbf{r},t) = -k_0^2 \exp(-j\omega_0 t) \int_{V_P} d\mathbf{r}'\, n(\mathbf{r}',t)\, [\hat{\mathbf{q}} \times (\hat{\mathbf{q}} \times \mathbf{E}(\mathbf{r}'))]\, g(\mathbf{r},\mathbf{r}') \tag{2.7}$$

where $d\mathbf{r}' = dx'dy'dz'$, V_P is the volume occupied by the plasma electrons, $\hat{\mathbf{q}}$ is a unit vector pointing from the point $P'(\mathbf{r}')$ in the plasma to the observer at $P(\mathbf{r})$ and

$$g(\mathbf{r},\mathbf{r}') = \frac{-\exp(jk_0 |\mathbf{r} - \mathbf{r}'|)}{4\pi |\mathbf{r} - \mathbf{r}'|} \tag{2.8}$$

is the Green's function. Since $\mathbf{E}$ appears in the right side of Eq. (2.7) a closed form solution for the integral equation does not exist. A number of perturbation techniques for obtaining approximate solutions for $\mathbf{E}_s$ (specifically the Born and Rytov approximations) are discussed in Sec. 4.1.

For small angle forward scattering, the vector triple cross product in the integrand of Eq. (2.7) varies little over the scattering volume, taking an approximately constant value $-\mathbf{E}$. In this approximation the electric field can be treated as a scalar quantity. The conditions under which this simplification is valid have been considered by [CLIFFORD (1978), LEE and HARP (1969), STROHBEHN (1968)]. Writing $\mathbf{E}(\mathbf{r},t) = \hat{\mathbf{E}}_0\, u(\mathbf{r},t)$ where $\mathbf{E}_0 = |\mathbf{E}_0|\, \hat{\mathbf{E}}_0$, the total scalar electric field becomes

$$u(\mathbf{r},t) = u_o(\mathbf{r},t) + u_s(\mathbf{r},t) \tag{2.9}$$

[3] hereafter simply referred to as the density

where the incident field $u_0(\mathbf{r},t) = u_0(\mathbf{r})\exp(-j\omega_0 t)$ satisfies the free space scalar Helmholtz equation and the scattered field

$$u_s(\mathbf{r},t) = \int_{V_p} d\mathbf{r}'\, f(\mathbf{r}',t)\, g(\mathbf{r},\mathbf{r}'). \tag{2.10}$$

is the solution to the scalar inhomogeneous Helmholtz equation with scattering potential

$$f(\mathbf{r},t) = k_0^2 n(\mathbf{r},t) u(\mathbf{r},t). \tag{2.11}$$

3 FREE SPACE PROPAGATION

For arbitrary incident radiation propagating in the positive z direction with wavenumber k_0 the wave field u_0 in the plane $z = 0$ can be decomposed into its incident "angular spectrum" [GOODMAN (1968)]:

$$A_0(k_x, k_y; 0) = \iint_{-\infty}^{\infty} u_0(x_i, y_i; 0) \exp\left[-j(k_x x_i + k_y y_i)\right] dx_i dy_i \tag{3.1}$$

$$\triangleq A_i(k_x, k_y) \tag{3.2}$$

where x_i and y_i denote spatial co-ordinates in the incident plane (here taken as $z = 0$ and denoted by subscript "i"), (k_x, k_y) are wavenumbers in the spatial frequency plane and the time dependence has been ignored. Satisfaction of the wave equation requires that the Fourier amplitudes A_0 satisfy a second order ordinary differential equation whose solution in some plane z can be expressed in terms of the angular components A_i at the incident plane as

$$A_0(k_x, k_y; z) = \mathcal{H}(k_z; z) A_i(k_x, k_y) \tag{3.3}$$

where

$$\mathcal{H}(k_z; z) = \exp(jk_z z) \tag{3.4}$$

is the free space transfer function or propagator [SHEWELL and WOLF (1968)] and the component of wave vector k in the z direction is given by

$$k_z = (k_0^2 - k_x^2 - k_y^2)^{1/2}. \tag{3.5}$$

The operator $\mathcal{H}$ can be regarded as a linear, dispersive, finite bandwidth spatial filter. For $k_x^2 + k_y^2 > k_0^2$, k_z is imaginary and the wave is evanescent. In Sec. 4 we derive a similar expression for the scattered wave field.

The free space field at some arbitrary plane z can be obtained from the incident angular spectrum $A_i(k_x, k_y)$ by taking the inverse two dimensional Fourier transform of the transfer function relation Eq. (3.3). If A_i consists of a single component (k_{0x}, k_{0y}), of amplitude a_0, the disturbance at $P(\mathbf{r})$ is given by

$$u_0(\mathbf{r},t) = a_0 \exp\left[j(\mathbf{k}_0 \cdot \mathbf{r} - \omega_0 t)\right] \tag{3.6}$$

which is a plane wave propagating with direction cosines $\mathbf{k}_0/k_0 = \left(k_{0x}, k_{0y}, (k_0^2 - k_{0x}^2 - k_{0y}^2)^{1/2}\right)/k_0$.

The amplitudes A_0 are mixed space and wavenumber quantities. The full three dimensional transform of an arbitrary incident field is given by

$$U_0(\mathbf{k}) = 2\pi A_i(k_x, k_y)\, \delta[k_z - (k_0^2 - k_x^2 - k_y^2)^{1/2}] \tag{3.7}$$

where δ represents the Dirac delta function. A single plane wave is represented by a point on a sphere in reciprocal space (the Ewald sphere) which is centered on the origin and has radius k_0.

4 THE DIFFRACTED WAVE FIELD

We now seek an equivalent wavenumber space representation to Eq. (3.3) for the scattered wave amplitude. The desired relation, given first by WOLF (1969) and known as the *diffraction projection theorem*, expresses the angular spectrum of the scattered radiation in terms of the Fourier transform of the scattering potential. For the special case of plane wave illumination, and in the limit of zero wavelength, the result reduces to the well known "central slice" theorem for non-diffracting tomographic imaging. The proof of the diffraction projection theorem rests on the assumption that the scattering is weak in a sense to be made clear below.

Although the solution Eq. (2.7) to the inhomogeneous wave equation contains the unknown scattered field on both sides, when the medium is "weakly fluctuating", an approximate solution can be obtained using perturbation techniques. Two widely employed and successful approaches are the *Born* approximation which expands the wave field in series form:

$$u = u_0 + u_1 + u_2 + \ldots \tag{4.1}$$

and the *Rytov* expansion, in which it is the exponent of u that is developed as a series:

$$u = \exp(\psi_0 + \psi_1 + \psi_2 + \ldots). \tag{4.2}$$

The Born approximation represents an additive perturbation of the incident field while the Rytov expansion is multiplicative in nature. It will be shown in Sec. 4.1 that the first order Rytov solution includes the Born approximation as a special case, but in many circumstances yields a superior solution for the scattered wave amplitude [ISHIMARU (1978)]. Perhaps more importantly, however, the validity of the solution is subject to considerably less stringent conditions on the strength of the scattering medium than its Born counterpart [GOODMAN (1985)].

The diffraction projection theorem is the wavenumber space solution to the inhomogeneous Helmholtz equation in the first order Born approximation and is discussed in Sec. 4.2.

4.1 The Weak Fluctuation Approximation

Keeping terms only up to first order in the Born expansion Eq. (4.1) and substituting into the scalar inhomogeneous wave equation gives [TATARSKI (1967)]:

$$(\nabla^2 + k_0^2)u_1 = k_0^2 n u_0 \tag{4.3}$$

where the second order term $k_0^2 n u_1$ can be neglected provided that $|u_1/u_0| \lesssim n$. To appreciate the meaning of this approximation, consider the wave to be normally incident upon a plasma "blob" of dimension $\sim \Lambda$ and density $n = n_e/n_{cr}$. The difference in phase between the incident (u_0) and transmitted ($u_0 + u_s$) beams is $\Delta\phi = (k - k_0)\Lambda$ where $k \sim k_0(1 - n/2)$ is the wavenumber in the plasma. In order that u_s be small we must have $\Delta\phi \ll \pi$ requiring that

$$n \ll K/k_0 \tag{4.4}$$

where $K = 2\pi/\Lambda$. The maximum tolerable density perturbation therefore depends upon the dimension of the inhomogeneity.

The first order solution to the inhomogeneous wave equation is given by

$$u_1(r,t) = \int_{-\infty}^{\infty} dr'\, f_1(r',t)\, g(r,r') \tag{4.5}$$

with

$$f_1(r,t) = k_0^2 n(r,t) u_0(r,t) \tau(r). \tag{4.6}$$

The integral limits in Eq. (4.5) have been extended to infinity through the introduction of the plasma volume function:

$$\begin{aligned} \tau(\mathbf{r}) &= 1 \qquad \mathbf{r} \in V_P \\ &= 0 \qquad \text{otherwise.} \end{aligned} \tag{4.7}$$

The solution is identical to Eq. (2.10) but for the replacement of $u(\mathbf{r}',t)$ by the incident field $u_0(\mathbf{r}',t)$ in the integrand (compare Eqs. (2.11) and (4.6)).

We now introduce the Rytov transformation (Eq. (4.2)) into the scalar wave equation and retain only terms up to first order in the complex phase ψ. The solution can be written as

$$u = u_0 \exp(\psi_1) \tag{4.8}$$

with the incident wave given by $u_0 = \exp(\psi_0)$. It can be verified that ψ_1 must satisfy the first order equation:

$$\nabla^2\psi_1 + 2\nabla\psi_0.\nabla\psi_1 = k_0^2 n(\mathbf{r},t)\tau(\mathbf{r}) \tag{4.9}$$

where the term $(\nabla\psi_1)^2$ has been neglected. Omitting this quantity is valid provided

$$(\nabla\psi_1)^2 << k_0^2 n. \tag{4.10}$$

For our plasma "blob" we take $|\nabla\psi_1| \sim \Delta\phi/\Lambda$ and the above condition becomes

$$n \ll 1 \tag{4.11}$$

which is independent of the scale size of the inhomogeneities. The Rytov approximation would certainly appear to be superior to its Born counterpart for forward angle scattering applications, and especially interferometry, where the condition $K/k_0 < 1$ is strongly satisfied. A useful comparison of the limitations of the two approximations in diffraction tomography applications is given by [SLANEY, KAK and LARSEN, (1984)]. The solution to Eq. (4.9) for the first order Rytov phase can be obtained as [ISHIMARU (1978)]:

$$\begin{aligned} \psi_1 &= \frac{u_1}{u_0} \\ &= \frac{1}{u_0(\mathbf{r})} \int_{-\infty}^{\infty} d\mathbf{r}'\, f_1(\mathbf{r}',t)\, g(\mathbf{r},\mathbf{r}'). \end{aligned} \tag{4.12}$$

In this paper we consider the plasma to be weakly fluctuating in the sense defined by either Eq. (4.4) or Eq. (4.11) so that only *first order* approximations to the scattered field u_s or Rytov phase ψ are necessary. We therefore take $u_s \equiv u_1$, $\psi_s \equiv \psi_1$ and $f \equiv f_1$ with the total scattered field in the Born approximation given by

$$u_B = u_0 + u_s, \tag{4.13}$$

and for the Rytov approximation

$$\begin{aligned} u_R &= u_0 \exp(\psi_s) \\ &= u_0 \exp\left(\frac{u_s}{u_0}\right). \end{aligned} \tag{4.14}$$

Clearly, any valid result for u_s can be extended to the first order Rytov solution ψ_s through the relation Eq. (4.14). In fact, the first two terms in the expansion of the exponential factor in Eq. (4.14) give the Born solution Eq. (4.13). The Rytov solution is generally regarded as superior to its Born counterpart, however, because of the higher order terms contained in the exponential.

4.2 Measured signals and the Rytov Phase

The phases ψ_0 and ψ_s are, in general, complex quantities. For example, for an incident plane wave, the complex phase can be written as $\psi_0 = \chi_0 + j\varphi_0$ where $\chi_0 = \ln a_0$ (the log-amplitude) and $\varphi_0 = \mathbf{k}_0.\mathbf{r} - \omega_0 t$ (total phase). The real and imaginary parts of ψ_s can be obtained from the first order solution Eq. (4.14) as

$$\begin{aligned} \chi_s + j\varphi_s &= \ln\left(\frac{u_R}{u_0}\right) \\ &= \ln\left(\frac{a_R}{a_0}\right) + j(\varphi_R - \varphi_0) \end{aligned} \tag{4.15}$$

where a_R and φ_R are the amplitude and phase of the field u_R. We now relate ψ_s to quantities which can be measured experimentally.

Mixing of the scattered light amplitude u_R with a suitably chosen local oscillator in a non-linear (square-law) detecting element can be used to produce measureable photo-currents [HOLZHAUER and MASSIG (1978)] that can be related to the properties of the scattered field. For simplicity, assume a local oscillator related to the incident field $u_0(\mathbf{r})\exp(-j\omega_0 t)$ by

$$u_{LO}(\mathbf{r}, t) = \alpha u_0(\mathbf{r})\exp -j(\omega_{LO}t + \phi_{LO}). \tag{4.16}$$

Here α is the ratio of the wave amplitudes, $\omega_{LO} = \omega_0 - \Omega_{LO}$ is the local oscillator frequency with $\Omega_{LO} \ll \omega_0$ the intermediate frequency and ϕ_{LO} is an arbitrary constant phase difference. The detected photo-current is proportional to the intensity $|\, u_R + u_{LO}\,|^2$ which has a time varying component

$$i = i_0\left[\exp(2\chi_s) + 2\alpha\exp(\chi_s)\cos(\varphi_s - \Omega_{LO}t - \phi_{LO})\right] \tag{4.17}$$

where $i_0(\mathbf{r}) = |\, u_0(\mathbf{r})\,|^2$ is the incident beam intensity. We immediately note that in the absence of a local oscillator beam (homodyne detection), only intensity fluctuations arising from the diffraction of the phase perturbed incident beam are observable:

$$i = i_0\exp(2\chi_s) = a_R^2. \tag{4.18}$$

On the other hand, the phase φ_s can be determined free of contamination from amplitude fluctuations when either χ_s is small or $\Omega_{LO} \gg \Omega$ where Ω represents a typical plasma component frequency. In the latter case, φ_s can be recovered at the zero crossings of $i(\mathbf{r}, t)$.

For the phase scintillation interferometer [NAZIKIAN and SHARP (1987)], $\Omega_{LO} = 0$, $\phi_{LO} = \pi/2$ and provided $|\chi_s|, |\varphi_s| \ll 1$, the fluctuating part of the detected signal is

$$i = 2i_0[\chi_s + \alpha\varphi_s]. \tag{4.19}$$

In this case, unless either diffraction effects are small $|\chi_s| \ll |\varphi_s|$ or the local oscillator is strong $\alpha \gg 1$, intensity variations can significantly affect the measured signal.

Clearly, the real and imaginary parts of ψ_s in the weak scattering limit can be related to measured intensity and phase fluctuations on a coherent probing beam. Because of these properties, we make extensive use of the first order Rytov phase.

4.3 The Diffraction Projection Theorem

The diffraction projection theorem relates the three dimensional transform of a weakly scattering transparent medium to the k-space properties of the diffracted wave. This relationship allows the extraction of some three dimensional information about the refractive index distribution though, in general, many directions of illumination are required to accurately characterize the scattering medium.

The statement of the diffraction projection theorem for a weakly diffracting medium and for conditions under which the scalar wave equation is valid is:

The angular spectrum of the forward scattered field in some plane z outside the medium, gives the values of the three-dimensional Fourier transform of the scattering potential on a hemispherical surface in the spatial frequency domain.

We sketch the proof of the diffraction projection theorem below. The reader is referred to the original presentation by [WOLF (1969)] as well as works by [MUELLER *et al.* (1971) and KAK (1985)] for more comprehensive treatments. In the derivation that follows, we maintain the arbitrary nature of the incident field distribution. The more general result is then reduced to the special case of plane wave illumination of the plasma in Sec. 5 and to Gaussian beams in Sec. 7.

Now consider Eq. (4.5) for the scattered scalar electric field. For a point source at $P'(\mathbf{r}')$, the Green's function solution to the wave equation is a free space spherical wave expanding about P' (see Eq. (2.8)). The spherical wave has the following plane wave decomposition [BANOS,1966]:

$$g(\mathbf{r},\mathbf{r}') = \frac{-j}{2}\iint_{-\infty}^{\infty} \frac{dk_x\,dk_y}{(2\pi)^2 k_z} \exp\{j[k_x(x-x') + k_y(y-y') + k_z|z-z'|]\} \tag{4.20}$$

where $k_z = (k_0^2 - k_x^2 - k_y^2)^{1/2}$. Now let us choose the coordinate origin (incident plane) so that the plasma occupies the region $0 < z' < L$. This choice will prove convenient in the discussion to follow. Since we are only interested in forward scattered radiation, the measurement plane is chosen beyond the plasma ($z > L$). The diffraction geometry for incident plane wave illumination is illustrated in Fig. 1.

Now insert the above expression for g into Eq. (4.5) for u_s. Since f is zero when $z > L$ we may replace $|z - z'|$ by $z - z'$ to obtain after some rearrangement

$$u_s(\mathbf{r},t) = \frac{-j}{2}\iint_{-\infty}^{\infty} \frac{dk_x\,dk_y}{(2\pi)^2 k_z} \exp(j\mathbf{k}.\mathbf{r}) \int_{-\infty}^{\infty} dz'\, f(z',t)\exp(-j\mathbf{k}.\mathbf{r}'). \tag{4.21}$$

The rightmost integral is recognised as the spatial Fourier transform of the product of the plasma density distribution, the incident wave field, and the plasma volume function τ. The scattered wave field can be more compactly expressed as

$$u_s(\mathbf{r},t) = \frac{-j}{2}\iiint_{-\infty}^{\infty} \frac{dk_x\,dk_y\,d\omega}{(2\pi)^3 k_z} \exp[j(\mathbf{k}.\mathbf{r} - \omega t)]\, F(\mathbf{k},\omega) \tag{4.22}$$

where F denotes the Fourier transform of the scattering potential.

The main result follows easily by taking the two dimensional Fourier transform over x and y to obtain the angular spectrum of u_s in the plane z:

$$A_s(\kappa_x,\kappa_y,\omega;z) = \mathcal{G}(\kappa_z;z)\,F(\kappa,\omega) \tag{4.23}$$

where

$$\mathcal{G}(\kappa_z;z) = \frac{-j}{2}\frac{\exp(j\kappa_z z)}{\kappa_z} = \frac{-j}{2\kappa_z}\mathcal{H}(\kappa\ \ z) \tag{4.24}$$

is the two dimensional Fourier transform of the Green's function g with

$$\kappa = (\kappa_x,\kappa_y,\kappa_z) \qquad |\kappa| = k_0 \tag{4.25}$$

$$\kappa_z = (k_0^2 - \kappa_x^2 - \kappa_y^2)^{1/2}. \tag{4.26}$$

Notice that the transfer function $\mathcal{G}$ is the same as the free space propagator $\mathcal{H}$ (Eq. (3.4)) apart from an imaginary factor. Thus an angular spectral component of the total Born field can be expressed as

$$A_B(\kappa_x,\kappa_y,\omega;z) = \mathcal{H}(\kappa_z;z)\left[A_i(\kappa_x,\kappa_y,\omega) - \frac{j}{2\kappa_z}F(\kappa,\omega)\right] \tag{4.27}$$

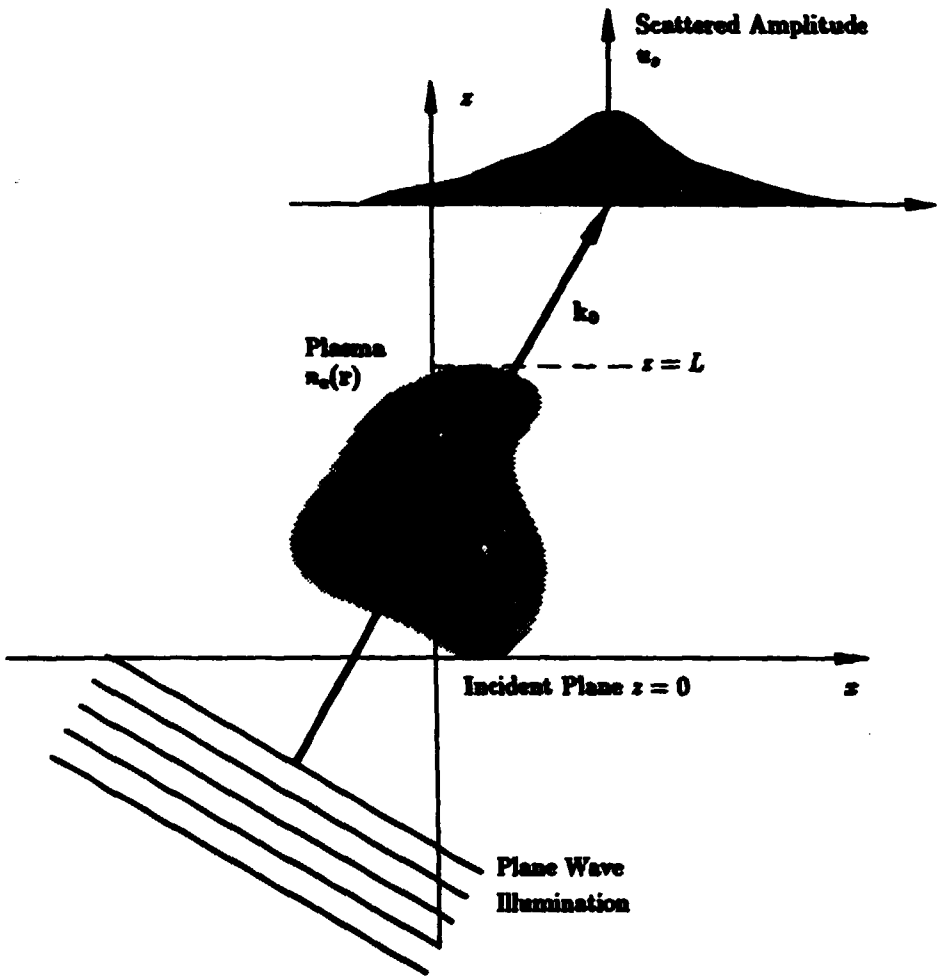

Figure 1: Diffraction geometry for the case of incident plane wave illumination of the plasma. The scattered wave field is measured in some arbitrary plane z.

where the vector κ represents the scattered wave vector. As κ_x and κ_y vary between $-k_0$ and k_0 (propagating components), the vector κ is confined to the hemispherical surface in reciprocal space that is centered on the origin and has radius k_0.

Suppressing, for the moment, the time dependence, the spatial Fourier transform of the scattering potential is given by the convolution theorem as

$$\begin{aligned} F(\kappa) &= \frac{1}{(2\pi)^3} k_0^2 \hat{N} * U_0(\kappa) \\ &= k_0^2 \int_{-\infty}^{\infty} \frac{d\mathbf{K}}{(2\pi)^3} \hat{N}(\mathbf{K})\, U_0(\kappa - \mathbf{K}) \end{aligned} \tag{4.28}$$

where U_0 is the Fourier transform of the incident field (Eq. (3.7)) and

$$\hat{N} = \frac{1}{(2\pi)^3} \mathcal{N} * T \tag{4.29}$$

is proportional to the three dimensional convolution of the transform $N = N_e/n_{cr}$ of the deterministic electron density distribution with the Fourier transform T of the plasma volume function

r. The wavenumber volume element is $d\mathbf{K} = dK_x\,dK_y\,dK_z$. When V_P is large compared with a typical fluctuation wavelength, T approaches a delta function distribution and $\hat{N} \to N$. The function T can be regarded as the point spread or wavenumber impulse response, and represents the maximum achievable wavenumber resolution of the scattering system. Notice that the wavenumber resolution is also degraded by an angular spread of incident wavenumbers.

Finally, when only a portion of the total Born scattered field is measured due to the presence of a an aperture in the detection plane, the computed angular spectrum Eq. (4.23) is a convolution of A_s with the transform $\Sigma(\kappa_x, \kappa_y; z)$ of the two dimensional aperture function $\sigma(x, y; z)$:

$$\hat{A}_s = \frac{1}{(2\pi)^2} A_s * \Sigma. \tag{4.30}$$

5 PLANE WAVE ILLUMINATION

Until now we have considered a general monochromatic incident field distribution. The expression for the scattered field becomes very simple when the incident radiation is the single plane wave component $\mathbf{k}_0 = (k_{0x}, k_{0y}, k_{0z})$ (c.f. Eq. (3.6)). In this case Eq. (4.23) reduces to a form similar to that first presented by [WOLF (1971)]:

$$A_s(\kappa_x, \kappa_y, \omega; z) = \mathcal{G}(\kappa_z; z)\, F_0(\boldsymbol{\kappa} - \mathbf{k}_0, \omega - \omega_0) \tag{5.1}$$

where the transform of the plane wave scattering potential is denoted F_0 and is given by

$$F_0(\mathbf{K}, \Omega) = k_0^2 a_0 \hat{N}(\mathbf{K}, \Omega) \tag{5.2}$$

and the density Fourier component is

$$(\mathbf{K}, \Omega) = (\boldsymbol{\kappa} - \mathbf{k}_0, \omega - \omega_0). \tag{5.3}$$

The result is illustrated in Fig. 2 for the $K_x K_z$ plane assuming $k_{0y} = 0$.

The forward scattered wave vector $\boldsymbol{\kappa}$ lies on a hemisphere which passes through the origin and has centre $(-k_{0x}, 0, -k_{0z})$. The axis of the hemisphere is in a direction normal to the measurement plane. The equation of the hemispherical surface is a restatement of the conservation of momentum relation Eq. (5.3) together with the condition $|\mathbf{k}_s| = |\mathbf{k}_0|$. The resulting vector relation is illustrated in the figure. The scattering angle θ_s is given by the familiar Bragg equation:

$$\sin\left(\frac{\theta_s}{2}\right) = \frac{K}{2k_0} \tag{5.4}$$

which for small angles becomes $\theta_s \simeq K/k_0$, $K = |\mathbf{K}|$.

An analogous k-space result can also be derived for the plane wave Rytov phase. Substituting Eqs. (3.6) and (4.21) for u_0 and u_s into expression Eq. (4.12) for ψ_s and Fourier transforming gives

$$\Psi_s(\kappa_x, \kappa_y, \Omega; z) = \mathcal{R}(\kappa_z; z)\hat{N}(\mathbf{K}, \Omega) \tag{5.5}$$

where we have introduced the Rytov phase propagator

$$\mathcal{R}(\kappa_z; z) = \frac{-jk_0^2}{2\kappa_z} \exp(jK_z z). \tag{5.6}$$

A strong similarity to the result for A_s is evident. Indeed, for plane wave illumination, the Fourier space relation between the Born and Rytov solutions is given by

$$\Psi_s = a_0 \exp(-jk_{0z} z)\, A_s \tag{5.7}$$

where we have used the relation $\kappa_z = k_{0z} + K_z$ (Eq. (5.3)).

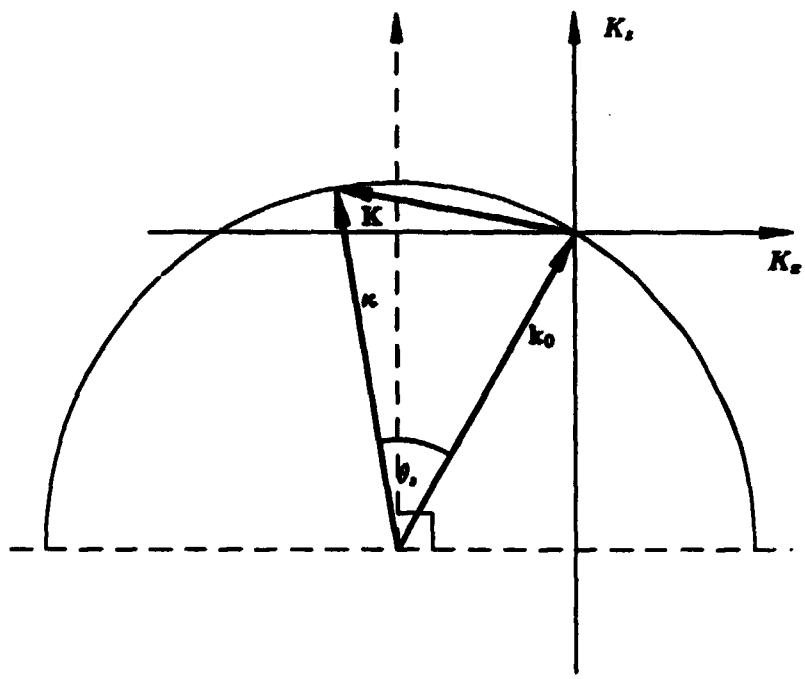

Figure 2: Schematic diagram showing the semi-circular slice in the Fourier transform plane K_xK_z along which the value of the transform of the plasma density distribution is determined by the angular spectrum A_s of the radiation scattered from an incident plane wave.

In principle A_s (or Ψ_s) can yield information about the electron density distribution to a wavenumber bandlimit of $2k_0$. By changing the angle of illumination (or detection), the entire transform up to this limit is accessible. In practice, a number of factors including restricted diagnostic access, reduce the available bandwidth, or allow only a small portion of the frequency plane to be examined. Diffraction tomography is of limited usefulness in such circumstances. More fundamentally, however, the condition under which Eq. (2.10) and hence the result Eq. (4.23) is valid, requires that the scattering angles be small enough that depolarisation effects can be ignored (scalar theory). We now consider the behaviour of the transfer functions $\mathcal{G}$, $\mathcal{H}$ and $\mathcal{R}$ for small scattering angles $\lesssim 30°$.

6 LIMITING FORMS OF THE DIFFRACTED FIELD

In Sec. 4.2 it was shown that the unperturbed (incident) and scattered angular spectra share the common propagator $\mathcal{H}(\kappa_z; z)$. We now indicate the *near field* limiting forms for the propagator and the simplifications to the theory that follow. Initially, we assume plane wave illumination $\mathbf{k} = (0, 0, k_0)$ of the scattering medium. The near field behaviour of the scattered field in the case of Gaussian beam illumination is examined in Sec. 7.

6.1 Parabolic Approximation

For small angle scattering κ_z for the scattered field can be approximated to second order by

$$\kappa_z \approx k_0 - \frac{K_x^2 + K_y^2}{2k_0} \triangleq \kappa_P. \tag{6.1}$$

This parabolic approximation to the hemispherical surface in k-space is illustrated in the $K_x - K_z$ plane in Fig. 4. The approximation is valid when the residual phase contribution from higher order terms is much less than one radian. This requires

$$k_0 z \ll (\Delta\Omega_K)^{-2} \tag{6.2}$$

where $\Delta\Omega_K$ is the solid angle of contribution of scattered radiation from the fluctuating component K at point $P(\mathbf{r})$ as depicted in Fig. 3. Since $\kappa_z = k_0 + K_z$, by analogy we write $\kappa_P = k_0 + K_P$ where

$$K_P = -(K_x^2 + K_y^2)/2k_0 = -2\pi/z_P \tag{6.3}$$

and z_P is the Fresnel length for diffraction from density perturbations of wavenumber $K_\perp = (K_x^2 + K_y^2)^{1/2}$.

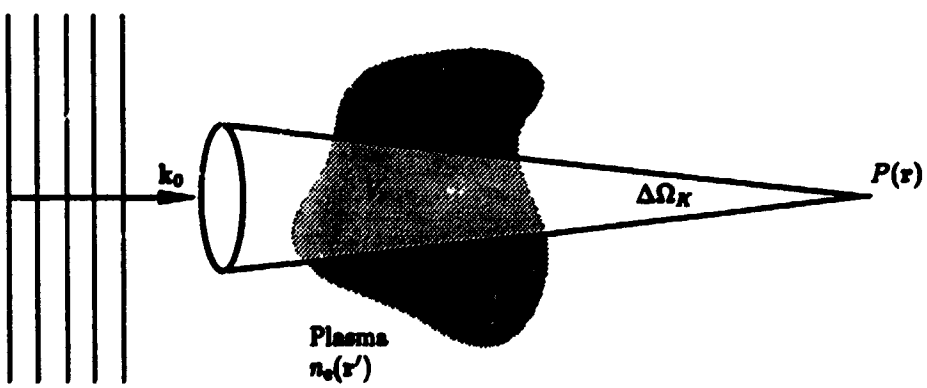

Figure 3: Cone of forward scattered rays received at the observation position P

The *near field* condition Eq. (6.2) is the same as that required for Fresnel approximation of the Green's function in the spatial domain. In the latter case, however, the solid angle subtended at P is determined by the dimensions of the scattering volume rather than the wavelength $\Lambda = 2\pi/K_\perp$ of the scattering fluctuation. When the near field condition is satisfied, the propagation transfer

functions are replaced by their parabolic approximations obtained by setting $\kappa_z = \kappa_P$ in the exponent and $\kappa_z = k_0$ in the denominator. For example, the Rytov phase propagator $\mathcal{R}$ becomes

$$\mathcal{R}_P(K_P; z) = \frac{-jk_0}{2} \exp(jK_P z). \tag{6.4}$$

The parabolic approximation to the *free space* field u_0 is obtained by inverse Fourier transform of Eq. (3.3) with $\mathcal{H}$ replaced by its Fresnel counterpart $\mathcal{H}_P$. By the convolution theorem

$$\begin{aligned} u_0(\mathbf{r}, t) &= u_i * h_P \\ &= \iint_{-\infty}^{\infty} u_0(x', y'; 0, t) h_P(x - x', y - y'; z) dx' dy' \end{aligned} \tag{6.5}$$

with the Fresnel kernel

$$h_P(x, y; z) = \frac{\exp(jk_0 z)}{j\lambda_0 z} \exp\left[\frac{jk_0}{2z}(x^2 + y^2)\right]. \tag{6.6}$$

The parabolic approximation is especially suited to the study of Gaussian beams which maintain their form under Fresnel transform.

The parabolic approximation to the *scattered field* can also be cast in a Fresnel integral form similar to Eq. (6.5) for the free space field. We prefer, however, to represent the scattered field as the superposition of beams identical to the incident field but diffracted from the medium at angles determined by the spectrum of the scatterer. The resulting expression, which is inspired by the well known Abbe diffration theory, is intuitively more appealing than the direct Fresnel integral, and serves as a platform for later work. We first isolate the incident field by combining Eqs. (4.22) and (4.28) to obtain

$$u_s(\mathbf{r}) = \frac{-jk_0^2}{2} \int_{-\infty}^{\infty} \frac{d\mathbf{K}}{(2\pi)^3} \hat{N}(\mathbf{K}) \iint_{-\infty}^{\infty} \frac{d\kappa_x d\kappa_y}{(2\pi)^2 \kappa_z} \exp(j\boldsymbol{\kappa}.\mathbf{r}) U_0(\boldsymbol{\kappa} - \mathbf{K}) \tag{6.7}$$

where, for notational ease, the time dependence has been suppressed. In the parabolic approximation the trajectory of the plane wave component $(0, 0, k_0)$ of the incident field diffracted from the perturbation $\mathbf{K}_P = (K_x, K_y, K_P)$ is

$$\tilde{\rho} = (\tilde{x}, \tilde{y}) = \left(x - \frac{K_x}{k_0}(z - z'), y - \frac{K_y}{k_0}(z - z')\right) \tag{6.8}$$

where, as usual, z' is the coordinate of the feature (K_x, K_y) in the plasma. Expanding U_0 using the Fourier representation Eq. (3.7), transforming to the more natural "trajectory" coordinates $(\tilde{x}, \tilde{y})$ and integrating then gives

$$u_s(\mathbf{r}) = \int_0^L dz' \iint_{-\infty}^{\infty} \frac{d\mathbf{K}_\perp}{(2\pi)^2} \exp(j\mathbf{K}_\perp.\boldsymbol{\rho}) \mathcal{R}_P(K_P; z - z') \hat{\mathcal{N}}(\mathbf{K}_\perp; z') u_0(\tilde{\rho}; z). \tag{6.9}$$

where we have introduced the notation $\mathbf{K}_\perp = (K_x, K_y)$, $\boldsymbol{\rho} = (x, y)$ and $d\mathbf{K}_\perp = dK_x dK_y$. We have also elected to write

$$\hat{\mathcal{N}}(\mathbf{K}_\perp; z') = \frac{1}{(2\pi)^2} \mathcal{N}(\mathbf{K}_\perp; z') * \Sigma_P(\mathbf{K}_\perp; z') \tag{6.10}$$

where $\mathcal{N}(\mathbf{K}_\perp; z')$ is the 1-D inverse Fourier transform of $N(\mathbf{K})$ and Σ_P is the two dimensional transform of the plasma aperture function $\sigma_P(\rho; z')$ at position z':

$$\begin{aligned} \tau(\mathbf{r}) &= \sigma_P(\rho; z)\, \Pi(z)\,; \\ \Pi(z) &= 1 \quad 0 < z < L \\ &= 0 \quad \text{otherwise.} \end{aligned} \tag{6.11}$$

The equivalent k–space representation for u_s can be obtained as

$$A_s(\varkappa_\perp, \omega; z) = \mathcal{G}_P(\varkappa_z; z)\, F(\varkappa_P, \omega) \tag{6.12}$$

where $\varkappa_P = (\varkappa_\perp, \varkappa_P)$ and $\mathcal{G}_P$ is the Fresnel approximation for $\mathcal{G}$. The correspondence with the more rigorous result Eq. (4.23) is clear.

Equation (6.9) indicates that corresponding to each density spectral component $\mathbf{K}_\perp$ there is a diffracted wave $u_0(\tilde{\rho}; z)$ identical in form to the incident field, and that the field u_s is the superposition of all such suitably weighted contributions. The power of the expression for evaluating the field scattered from a thin weakly diffracting phase screen is demonstrated in a later paper. The result also allows easy evaluation of the Rytov phase for Gaussian beam illumination as shown in Sec. 7.

With $\psi_s = \chi_s + j\varphi_s = u_s/u_0$, the real and imaginary parts of the plane wave Rytov phase can be obtained using Eq. (6.9):

$$\left.\begin{matrix}\chi_s(\mathbf{r}, t) \\ \varphi_s(\mathbf{r}, t)\end{matrix}\right\} = \int_0^L dz' \int_{-\infty}^{\infty} \frac{d\mathbf{K}_\perp}{(2\pi)^2} \exp(j\mathbf{K}_\perp \cdot \boldsymbol{\rho}) \mathcal{R}_{\substack{\chi \\ \varphi}}(K_P; z - z') \hat{N}(\mathbf{K}_\perp; z', t) \tag{6.13}$$

where we have defined

$$\mathcal{R}_\chi(K_P; z) = \frac{k_0}{2} \sin(K_P z) \tag{6.14}$$

$$\mathcal{R}_\varphi(K_P; z) = \frac{-k_0}{2} \cos(K_P z). \tag{6.15}$$

Fourier transformation of Eq. (6.13) gives the transfer function result

$$\Psi_s(\mathbf{K}_\perp, \Omega; z) = \mathcal{R}_P(K_P; z) \hat{N}(\mathbf{K}_P, \Omega). \tag{6.16}$$

This can be compared with the more general result Eq. (5.5) for the transform of the plane wave Rytov phase.

6.2 Raman-Nath Scattering

The k-space analysis of weak diffraction phenomena provides an intuitively very powerful tool for relating the scattered wave field to the structural properties of the plasma. Consider, for example, a quasi-monochromatic plasma wave propagating with mean wavenumber K_z in a slab of thickness Δz normal to the incident plane wave. This component is conveyed by the scattered field according to the strength its transform at the intersection with the circular arc defining the locus of allowable scattered wave vectors. Since the spectral width $\Delta K_z \sim 2\pi/\Delta z'$ represents the minimum distance over which the transform $\hat{N}$ can change significantly, the narrower the structure the greater will be the domain of its transform in the dimension K_z. Recalling that $0 < z' < L$ it is therefore sufficient that the inequality $|K_P|\Delta z' < |K_P| L \sim |K_P|/\Delta K_T \lesssim 1$ be satisfied for the density wave be sensed by the probing radiation (see Fig. 4). Here $\Delta K_T \sim 2\pi/L$ is the spectral width of the z-component of the point spread T.

When the quantity $Q = |K_P| L$ is sufficiently small the transform $\hat{N}(\mathbf{K})$ can be approximated to first order as

$$\hat{N}(\mathbf{K}_P, \Omega) \approx \int_0^L dz' (1 - jK_P z') \hat{N}(\mathbf{K}_\perp, \Omega; z'). \tag{6.17}$$

Q is the Klein-Cook parameter [KLEIN and COOK (1967)] and the Raman-Nath scattering regime occurs when $Q \ll 1$. The condition $Q \gg 1$ corresponds to Bragg scattering. Because $0 < L < z$ the Raman-Nath criterion is almost always well satisfied for near field scattering and interferometry experiments and in essence requires that amplitude fluctuations on the probing beam inside the plasma be negligible.

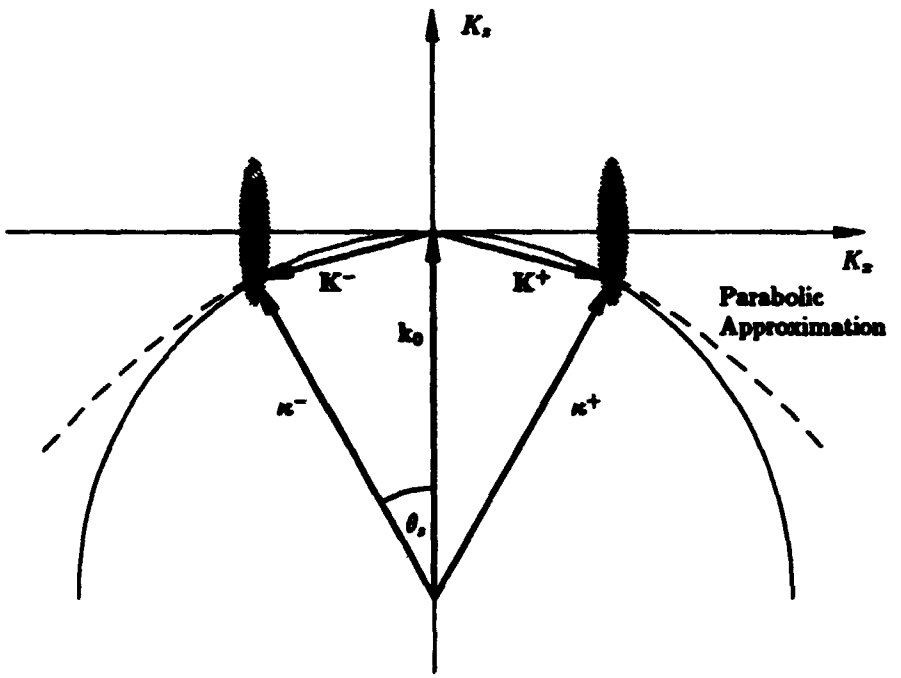

Figure 4: Schematic diagram showing the parabolic approximation to the semi-circular arc in the region of the origin for the case of an incident plane wave. The shaded areas show the dominant regions of the Fourier transform of a quasi-monochromatic plasma wave having $Q \lesssim 1$.

6.3 Geometric Optics

In the *geometric optics* approximation [TATARSKI (1967)] the *free space* transfer function $\mathcal{H}_P$ is expanded to first order as

$$\mathcal{H}_P(\kappa_P; z) \approx \exp(jk_0 z)(1 + jK_P z). \tag{6.18}$$

This approximation is valid whenever $|K_P|z \ll 1$, or alternatively, when

$$k_0 z \ll (\Delta\Omega_K)^{-1} \tag{6.19}$$

is satisfied (*c.f.* Eq. (6.2)). In the *ultra near field* terms of first order in $K_P z$ are also ignored so that diffraction effects are entirely negligible and the propagated free space field is identical to the incident field.

Now consider the behaviour of *scattered field* (as described by the plane wave Rytov phase) in this limit. Satisfaction of the condition Eq. (6.19) is obtained when the obeservation plane z is sufficiently close to the plasma or by restricting attention to small enough scattering wavenumbers. Since $0 < z' < z$, the geometric optics approximation necessarily implies diffraction in the Raman-Nath regime. Expanding the propagator $\mathcal{R}_P$ to first order in $K_P z$, and with the first order Raman-Nath approximation for $\hat{N}$, inverse Fourier transform over K_x, K_y and Ω gives for the imaginary part of ψ_s

$$\varphi_s(x,t) = -r_e\lambda_0 \int_0^L dz'\, n_e(x, y, z'; t). \tag{6.20}$$

where second order terms have been neglected. The effect of the higher order terms (diffraction) is examined in Sec. 9. The phase φ_s represents a retardation of u_R relative to the phase of the incident wave. The result is valid in the Rytov approximation which, assuming the medium

varies smoothly, can be written as $\varphi_s << k_0 L$ where the right hand side is the phase shift of the unperturbed wave. In absolute terms the phase φ_s can be large. The Fourier transform of φ_s gives the value of $\hat{N}$ in the plane $K_z = 0$. This is just a restatement of the well known "central slice" theorem for tomographic imaging [BRACEWELL (1979)] and the phase of the scattered field in the plane z is a geometric *projection* of the density distribution.

The Rytov phase has a real part which can be evaluated in a similar fashion as

$$\chi_s(\mathbf{r}) = \frac{1}{4n_{cr}} \int_0^L dz' (z - z') \nabla_\perp^2 n_e(x, y, z') \tag{6.21}$$

where

$$\nabla_\perp^2 = \left(\frac{\partial^2}{\partial x^2} + \frac{\partial^2}{\partial y^2} \right). \tag{6.22}$$

This term represents amplitude fluctuations arising as a result of diffraction and interference of the plane wave components constituting the total scattered wave field. Amplitude fluctuations are negligible in the ultra near field of the diffracting structure. Away from this region, however, the intensity scintillations can be measured (shadowgraph diagnostic technique) and related to the properties of the plasma.

7 GAUSSIAN BEAMS

In scattering experiments, the probing beam produced by a laser or solid state source almost invariably has a Gaussian power profile. The field distribution at the waist $z = z_0$ of such a beam propagating along the z-axis can be written [SIEGMAN (1971)]

$$u_G(\rho, z_0, t) = \frac{a_0}{\sqrt{\pi} w_0} \exp\left(-\frac{\rho^2}{2w_0^2} \right) \exp[j(k_0 z_0 - \omega_0 t)] \tag{7.1}$$

where w_0 is the beam half width at the $1/e$ point of the intensity profile [4]. Noting that $\rho = |\rho| \sim w_0$, and since the observation distance z is usually significantly greater than w_0, we obtain the propagated Gaussian beam in the parabolic approximation from the inverse Fourier transform of $\mathcal{H}_P A_G$ where A_G is the angular spectrum of the field at the waist. The propagated field is

$$u_G(\mathbf{r}, t) = \frac{a_0}{\sqrt{\pi} w_0} \gamma(z - z_0) \exp\left[-\frac{\rho^2}{2w_0^2} \gamma(z - z_0) \right] \exp[j(k_0 z - \omega_0 t)] \tag{7.2}$$

where we have defined

$$\gamma(z) = \frac{1 - jz/z_R}{1 + \delta^2/r_R^2} \tag{7.3}$$

and the Rayleigh length $z_R = k_0 w_0^2$ is the Fresnel length for diffraction from an aperture of width $\sim w_0$. It can be confirmed that $u_G(\rho, z + z_1) = h_P(\rho, z_1) * u_G(\rho, z)$ so that the Gaussian retains its form in the parabolic approximation.

An expression for the first order Gaussian beam Rytov phase ψ_G can be obtained by dividing Eqs. (6.9) and (7.2):

$$\psi_G(\mathbf{r}, t) = \int_0^L dz' \int_{-\infty}^{\infty} \frac{d\mathbf{K}_\perp}{(2\pi)^2} \exp(j\beta \mathbf{K}_\perp \cdot \rho) \, \mathcal{R}_G(K_P; z, z') \, \hat{N}(\mathbf{K}_\perp; z', t). \tag{7.4}$$

The Gaussian Rytov phase propagator

$$\mathcal{R}_G(K_P; z, z') = \frac{-jk_0}{2} \exp[j\beta(z, z') K_P(\mathbf{r} - \mathbf{r}')] \tag{7.5}$$

[4] The beam power is normalised for power flow $i_0 = a_0^2$

is identical to $\mathcal{R}_F$ but for a complex factor β that is given by

$$\beta(z,z';z_0) = \frac{[1-j(\zeta-\zeta_0)][1+j(\zeta'-\zeta_0)]}{1+(\zeta-\zeta_0)^2} \tag{7.6}$$

$$= \gamma(\zeta-\zeta_0)\,[1+j(\zeta'-\zeta_0)] \tag{7.7}$$

with normalised coordinates

$$\zeta = z/z_R \qquad \zeta' = z'/z_R \qquad \zeta_0 = z_0/z_R. \tag{7.8}$$

Equation (7.4) can also be cast in a convolution form analogous to the free space Fresnel transform:

$$\psi_G(\rho,z) = \int_0^L dz' \int_{-\infty}^{\infty} d\rho'\, h_G(\rho'-\beta\rho;z,z')\, u(\rho',z') \tag{7.9}$$

where

$$h_G(\rho;z,z') = -\frac{k_0^2}{4\pi\beta(z,z')(z-z')}\exp\left[j\frac{k_0\rho^2}{2\beta(z,z')(z-z')}\right] \tag{7.10}$$

is the Gaussian Fresnel kernel. Equations (7.4) and (7.10) have also been derived by [ISHIMARU (1969)]. For plane wave illumination $\beta(z,z';z_0)=1$ and Eq. (7.4) reproduces the plane wave Rytov phase Eq. (6.13). Separating ψ_G into its real and imaginary parts gives

$$\left.\begin{matrix}\chi_G(\mathbf{r},t)\\ \varphi_G(\mathbf{r},t)\end{matrix}\right\} = \int_0^L dz' \int_{-\infty}^{\infty} \frac{d\mathbf{K}_\perp}{(2\pi)^2}\mathcal{D}_{\substack{\chi\\ \varphi}}(\mathbf{K}_\perp;\rho,z,z')\,\hat{N}(\mathbf{K}_\perp;z',t) \tag{7.11}$$

where we have defined

$$\left.\begin{matrix}2\mathcal{D}_\chi(\mathbf{K}_\perp;\rho,z,z')\\ 2j\,\mathcal{D}_\varphi(\mathbf{K}_\perp;\rho,z,z')\end{matrix}\right\} = \exp(j\beta\mathbf{K}_\perp.\rho)\,\mathcal{R}_G(K_F;z,z') \pm \exp(j\beta^*\mathbf{K}_\perp.\rho)\,\mathcal{R}_G^*(K_F;z,z'). \tag{7.12}$$

Two important regimes of approximation for β are immediately apparent (see Fig. 5):

(i) $z'-z_0 \ll z_R$. In this case, the Gaussian waist lies in or near the plasma volume and the wavefront curvature in the plasma volume can be neglected (collimated beam). Provided z is not too large, $\beta(z,z';z_0)\to\gamma(z-z')$. This is the situation most frequently encountered in near field scattering and imaging experiments.

(ii) $z-z' \ll z_R$. In this limit $\beta\to 1$ and the Rytov phase ψ_G approaches the plane wave Rytov phase ψ_o irrespective of the position of the beam waist.

When both conditions (*i*) and (*ii*) are satisfied, the plasma and observation plane are within the collimated region of the beam and β may be approximated to first order in ζ and ζ' as $\beta\approx 1-j(\zeta-\zeta')$. Notice that this approximation restores the z shift invariances of the kernels $\mathcal{D}_\chi$ and $\mathcal{D}_\varphi$. With the additional reasonable assumption that measurements are performed within the most intense portion of the beam ($|\mathbf{K}_\perp.\rho| \lesssim K_\perp w_0$), we expand to first order in $K_G z \equiv K_\perp w_0(z/z_R)$

$$\exp(j\beta\mathbf{K}_\perp.\rho)\,\mathcal{R}_G(K_F;z) \approx \exp(j\mathbf{K}_\perp.\rho)\,\mathcal{R}_F(K_F;z)\left(1+\frac{\mathbf{K}_\perp.\rho}{z_R}z\right) \tag{7.13}$$

with the resulting approximations

$$\mathcal{D}_\chi(\mathbf{K}_\perp;\rho,z) = \frac{k_0}{2}\exp(j\mathbf{K}_\perp.\rho)\left[\sin(K_F z) - j\frac{\mathbf{K}_\perp.\rho}{z_R}z\cos(K_F z)\right] \tag{7.14}$$

$$\mathcal{D}_\varphi(\mathbf{K}_\perp;\rho,z) = \frac{-k_0}{2}\exp(j\mathbf{K}_\perp.\rho)\left[\cos(K_F z) + j\frac{\mathbf{K}_\perp.\rho}{z_R}z\sin(K_F z)\right]. \tag{7.15}$$

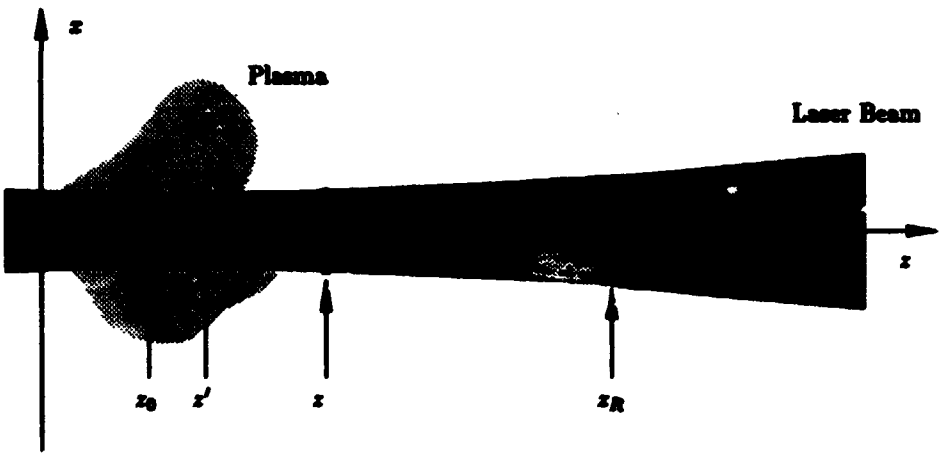

Figure 5: Collimated Gaussian beam probing of a plasma showing the relative positions of the waist (z_0), a point in the plasma (z'), the detection plane (z) and the Rayleigh range (z_R, measured from z_0). The figure dimensions are not to scale.

The condition

$$K_G z \sim \frac{z}{(z_R z_P)^{1/2}} \ll 1 \tag{7.16}$$

is interpreted pictorially in Fig. 6 and will be termed the *Gaussian near field*. Observe that for $z_R \sim z_P$ the restriction is identical to the geometric optics condition $K_P z \ll 1$.

Assuming that $K_P z \lesssim 1$ (this constraint is not so strong as the geometric optics condition), the ratio of the terms on the right side of Eq. (7.15) is of order $(K_G z)(K_P z) \ll 1$. The second term in $\mathcal{D}_\varphi$ can therefore be neglected and the plane wave result Eq. (6.13) for the phase perturbation is recovered in the Gaussian near field. On the other hand, for $\mathcal{D}_\chi$, the second term is negligible only when $K_G/K_P = (z_P/z_R)^{1/2} \ll 1$. An explicit expression can be obtained for χ_G in the limit of geometric optics $z \ll z_P$. Expanding the kernel $\mathcal{D}_\chi$ to first order in $K_P z$ and substituting into Eq. (7.11) gives

$$\chi_G(\mathbf{r},t) = \frac{1}{4}\int_0^L dz'(z-z')\left(\nabla_\perp^2 n - \frac{1}{w_0^2}\boldsymbol{\rho}.\nabla_\perp n\right) \tag{7.17}$$

which, as already noted, reduces to its plane wave counterpart Eq. (6.21) when $z_P \ll z_R$.

8 INTERFEROMETRY

An interferometer may employ either a single expanded Gaussian beam to illuminate part or all of the plasma cross section in a given plane, or use an array of discrete probing beams. In either case, though it is valid to take $\varphi_G = \varphi$, in the Gaussian near field (provided $K_P z \lesssim 1$), the measured beam intensity $i_G = u_G u_G^*$ is quite different from that for the ideal case of plane wave illumination due to the spatially apodising effects of the beam profile. It is therefore instructive to examine the *k-space properties* of the time varying part of the diffracted field intensity (see Eq. (4.17)) measured by the interferometer. To this end we consider detected signals in the limit of small phase and amplitude perturbations.

The fluctuating component can be expressed as (c.f. Eq. (4.19))

$$i = 2i_0 i_G(\chi_G + \alpha\varphi_G) \tag{8.1}$$

where $i_G = u_G u_G^*/i_0$ is the normalised intensity profile of the combined incident and local oscillator beams and $i_0 = a_0^2$. The above is appropriate for the scintillation diagnostic, a high sensitivity Mach-Zehnder heterodyne interferometer which operates in the geometric optics (Raman-Nath) regime [NAZIKIAN and SHARP (1987)]. Since both real and imaginary parts of ψ_G figure in this expression, let us for the moment consider the normalised complex "intensity"

$$c = i_G\psi_G. \tag{8.2}$$

Upon substitution for u_G, we can derive the following, rather cumbersome expression for the spectrum of c :

$$\begin{aligned} C(\mathbf{K}_\perp,\Omega;z) &= \frac{-jk_0}{2} I_G(\mathbf{K}_\perp;z)\int_0^L dz' \int_{-\infty}^{\infty} \frac{d\mathbf{K}'_\perp}{(2\pi)^2} \\ &\times \exp[-z_R(1+\tilde{\zeta}^2)\beta(z,z')K^*]\hat{N}(\mathbf{K}'_\perp,\Omega;z')\, I_G(\mathbf{K}'_\perp;z') \end{aligned} \tag{8.3}$$

where

$$I_G(\mathbf{K}_\perp;z) = \exp[-K_\perp^2 w_0^2(1+\tilde{\zeta}^2)/4] \tag{8.4}$$

is the two dimensional spatial Fourier transform of the field intensity profile i_G and we have written $\tilde{\zeta} = \zeta - \zeta_0$. We have also denoted by K^* the wavenumber quantity $-\mathbf{K}'_\perp.\mathbf{K}_\perp/2k_0$.

8.1 Discrete Chord Interferometry

Now consider the simple case where most of the beam energy is collected using a focussing lens and measured by a single detecting element. This corresponds to the standard case of discrete chord interferometry:

$$\tilde{i}(\Omega;z) = \int_{-\infty}^{\infty} d\rho\, \sigma_D(\rho,z)\, i_G(\rho,z)\, \varphi_G(\Omega;\rho,z). \tag{8.5}$$

Assuming that the collecting aperture $\sigma_D(\rho,z)$ is large compared with the beam dimensions we may write with little error

$$\begin{aligned} \tilde{i}(\Omega;z) &= \Re[C_\Phi(0,\Omega;z)] \\ &= \frac{-k_0}{2}\int_0^L dz' \int_{-\infty}^{\infty} \frac{d\mathbf{K}'_\perp}{(2\pi)^2} \hat{N}(\mathbf{K}'_\perp,\Omega;z')\, I_G(\mathbf{K}'_\perp;z') \end{aligned} \tag{8.6}$$

where C_Φ is the anti-Hermitian part of the transform C given by Eq. (8.3). It is interesting to note that the contribution from the amplitude perturbations averaged over the beam area is zero ($C_\chi = 0$).

Because of the diffraction and subsequent loss of high K information from the most intense portion of the Gaussian beam envelope, the probing beam acts as a low pass filter for transmission of line integrated refractive index information When $\tilde{\zeta}' \ll 1$ the filter bandwidth is $\sim 2/w_0$. The fluctuating signal can also be expressed as (c.f. Eq. (6.20))

$$\tilde{i}(\Omega;z) = -r_e\lambda_0 \int_0^L dz'\, \tilde{n}_e(0,0,z') \tag{8.7}$$

where $\tilde{n}_e(0,0,z')$ is the filtered density on axis of the beam probe. Observe that the validity of this result does not require satisfaction of the geometric optics condition. It would appear that an approximately bandlimited picture of the plasma profile can be produced by a set of sufficiently closely spaced discrete probing beams. This principle is exploited in a novel interferometer arrangement proposed by [HOWARD (1989)].

8.2 Expanded Beam Interferometry

Now we examine the case where the 2-D scattered field from a single (expanded) probing beam is sampled in the Gaussian near field using a linear detector array aligned in the z direction with centre at $(0,0,z)$ (coincident with the axis the incident Gaussian beam). We evaluate the detected intensity spectrum in the case when both plasma and observer lie within the collimated portion of the probing beam (conditions (*i*) and (*ii*) apply). Once again $\beta(1+\tilde{\zeta}^2) = (1-j\tilde{\zeta})(1+j\tilde{\zeta}') \rightarrow 1 - j(\zeta - \zeta')$ and Eq. (8.3) becomes

$$C(\mathbf{K}_\perp, \Omega; z) = \exp\left[-(K_G z)^2/4\right] \int_{-\infty}^{\infty} \frac{d\mathbf{K}'_\perp}{(2\pi)^2} \mathcal{R}_P(K^*; z)\, I_G(\mathbf{K}'_\perp - \mathbf{K}_\perp; 0)\, \hat{N}(\mathbf{K}'_\perp, K^*; \Omega). \tag{8.8}$$

Observe that the term I_G significantly weights the integral for wavenumbers $|\mathbf{K}'_\perp - \mathbf{K}_\perp| \lesssim 2/w_0$. For values of $\mathbf{K}'_\perp$ satisfying this inequality we can expand the exponent $K^* z$ as

$$\begin{aligned} K^* z = -\frac{\mathbf{K}'_\perp . \mathbf{K}_\perp}{2k_0} z &= K_P z - \frac{\mathbf{K}_\perp . (\mathbf{K}'_\perp - \mathbf{K}_\perp)}{2k_0} z \\ &\approx K_P z \end{aligned} \tag{8.9}$$

provided that

$$\frac{|\mathbf{K}_\perp . (\mathbf{K}'_\perp - \mathbf{K}_\perp)|}{2k_0} z \leq \frac{K_\perp\, |\mathbf{K}'_\perp - \mathbf{K}_\perp|}{2k_0} z \lesssim K_G z \ll 1 \tag{8.10}$$

and Eq. (8.8) reduces to the convolution

$$C(\mathbf{K}_\perp, \Omega; z) = \mathcal{R}_P(K_P; z) \exp\left[-(K_G z)^2/4\right] \left[\frac{1}{(2\pi)^2} (\hat{N} * I_G)(\mathbf{K}_P; \Omega)\right]. \tag{8.11}$$

The final inequality above is, of course, the Gaussian near field condition Eq. (7.16).

Again, the Gaussian factor in Eq. (8.11) damps the high wavenumber contribution to the spectrum. In the Gaussian near field, however, this bandlimiting is a second order effect and is neglected. The transform of the Gaussian intensity profile also smooths the plasma density spectrum in a fashion analogous to the transform $\Sigma_P(\mathbf{K}_\perp; z)$ of the 2-D plasma window function $\sigma_P(\rho; z)$ (see Eq. (8.10)). From a practical viewpoint, however, it is the Gaussian envelope which is often the most important aperture. Its effect, represented by the 2-D convolution, is hereafter represented by the $\hat{}$ superscript. The Gaussian near field result can therefore be more concisely written as

$$C(\mathbf{K}_\perp, \Omega; z) = \mathcal{R}_P(K_P; z) \hat{\hat{N}}(\mathbf{K}_P; \Omega). \tag{8.12}$$

Because of the essentially identical nature of Eqs. (8.12) and (6.16) the Raman-Nath and geometric optics approximations derived for the plane wave Rytov phase can be trivially extended to the case of beam illumination in the Gaussian near field. Equation (8.12) could also have been obtained directly in the spatial domain by noting that in the ultra near field, $\psi_G \rightarrow \psi_s$ and the measured photo-current is proportional to the plane wave Rytov phase weighted by the intensity of the Gaussian beam. This is the basis of the phase scintillation diagnostic method described by [SHARP (1983) and JAMES and YU (1985)].

For line integral measurements in a poloidal plane it is an excellent approximation to ignore the variation of n in the toroidal direction and so represent the plasma spectrum as $\hat{N} = 2\pi \hat{N}(K_x; z')\delta(K_y)$. Convolution with the Gaussian I_G then gives

$$\hat{\hat{N}}(K_x, K_y; z') = \exp\left(-K_y^2 w_0^2/4\right) \hat{N}(K_x; z'). \tag{8.13}$$

The 2-D photo-current spectrum is also degraded by convolution with the wavenumber response of the linear detetector array (*c.f.* Eq. (4.30)). We assume the array has linear extent $D \gtrsim 2w_0$ so

that the additional blurring $\Sigma_D * C$ in the direction K_x can be ignored. In the geometric optics approximation, such a linear detector array gives for the phase component

$$\hat{C}_\Phi(K_x, y, \Omega) = \frac{-jk_0}{2} \int_0^L dz' \int_{-\infty}^{\infty} \frac{dK_y}{2\pi} \exp(jK_y y) \hat{\tilde{N}}(K_x, K_y, \Omega; z'). \tag{8.14}$$

An analogous expression is obtained for $\hat{C}_X$. Substituting for $\hat{\tilde{N}}$ from Eq. (8.13) and performing the integral yields

$$\hat{C}_\Phi(K_x, 0; \Omega) = \frac{-jk_0}{w_0(4\pi)^{1/2}} \int_0^L dz' \hat{\tilde{N}}(K_x, \Omega; z'). \tag{8.15}$$

As expected, he measurements again yield a geometric projection of the 1-D plasma density profile, and the intensity at the detector is inversely proportional to the waist dimension in the direction orthogonal to the measurement array.

It is clearly desirable to take advantage of the simple relationships between detected signals and the plasma structure offered in the geometric optics approximation. In situations where the detecting plane must be remote from the plasma, these conditions can be restored using imaging techniques [HUGENHOLTZ and MEDDENS (1962), YOUNG *et al.* (1964), HOWARD *et al.* (1967), NAZIKIAN and SHARP (1967)]. When the beam is allowed to freely propagate before being sensed by an array of detectors [e.g. PEEBLES *et al.* (1967), KIM *et al.* (1968)] the effects of the propagation transfer function $\mathcal{R}_P$ must be carefully assessed.

8.3 Imaging Interferometry

When diffraction of the probing beam is important, a lens system can be used to produce an image of the ultra near field diffracted light amplitude in the detector plane. Consider an incident Gaussian beam diffracting from a plasma wave located in some object plane ($z = 0$) at distance d_0 in front of an infinite aperture thin lens (see Figs. 4 and 6). Allow the light to propogate through the lens to an arbitrary detecting plane at distance d_1 behind the lens. For a well collimated beam and small scattering angles the infinite aperture assumption is a reasonable approximation.

The field u_1 in the detecting plane $z_1 = d_0 + d_1$ is given in the Fresnel approximation by:

$$u_1(x_1, y_1, z_1) = \iint_{-\infty}^{\infty} dx_0 dy_0 \, h_L(x_0, y_0; x_1, y_1; d_0, d_1) u_0(x_0, y_0; 0) \tag{8.16}$$

where the lens kernel h_L is given by

$$h_L = \alpha \exp(j\phi_L) \, h_P(x_0 - \alpha x_1, y_0 - \alpha y_1; d_0 + \alpha d_1) \tag{8.17}$$

with

$$\alpha = 1/(1 - d_1/f) \tag{8.18}$$

$$\phi_L(x_1, y_1; d_1) = -\frac{k_0 \alpha}{2f}(x_1^2 + y_1^2 + 2d_1^2) \tag{8.19}$$

and h_P is the Fresnel kernel given by Eq. (6.6). Apart from the phase and scaling terms, the operation of the lens is to produce a Fresnel transform. This is especially useful for Gaussian beam scattering from thin phase screens where analytic solutions can be found.

Substituting the imaging condition $\alpha = -d_0/d_1$ in the expression Eq. (8.17) for h_L yields for the detected field in the image plane:

$$u_1(x_1, y_1, z_1) = -\frac{1}{M} u_0\left(-\frac{x_1}{M}, -\frac{y_1}{M}; 0\right). \tag{8.20}$$

This is a scaled and inverted image of the scattered beam in the ultra near field (no diffraction effects) with magnification factor $M = -1/\alpha$. In this result we have omitted the unimportant

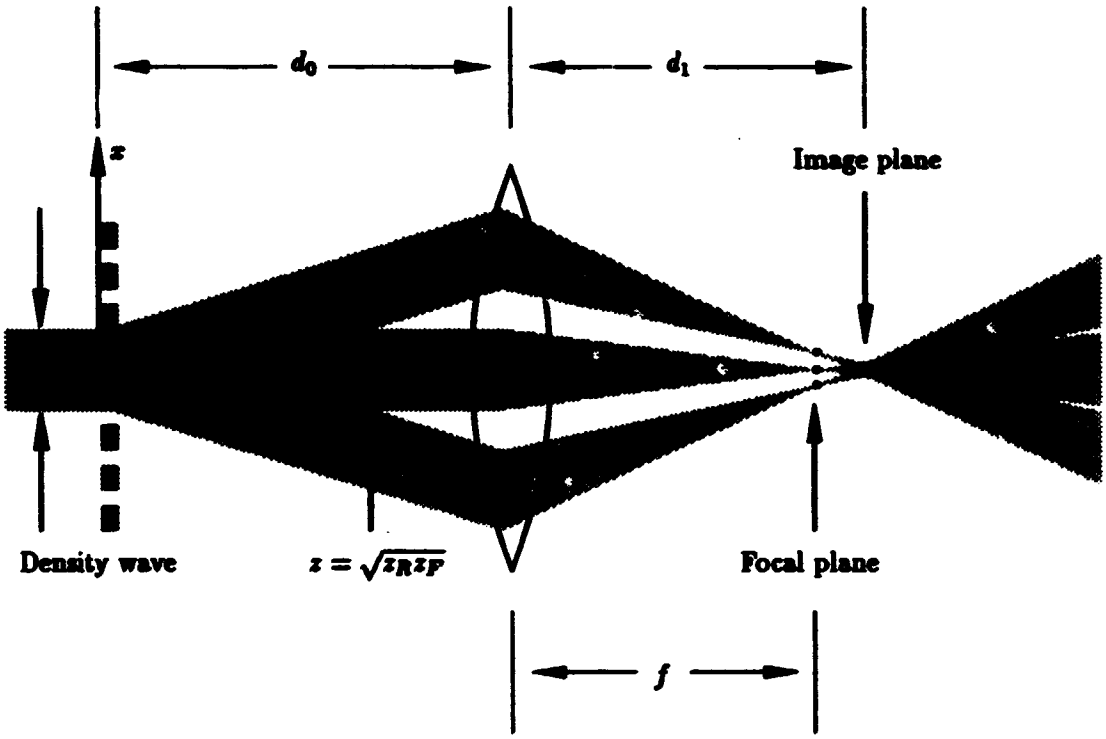

Figure 6: Imaging of the field diffracted from a density wave for incident collimated Gaussian beam illumination.

phase term ϕ_L. Though spatially varying, ϕ_L is constant in time and is hereafter neglected. In wavenumber space Eq. (8.16) can be cast in the form

$$A_1(\alpha\kappa_x, \alpha\kappa_y; z_1) = \frac{1}{\alpha}\mathcal{H}_P(\kappa_P; d_0 + \alpha d_1) A_0(\kappa_x, \kappa_y; 0). \tag{8.21}$$

It is straightforward to then compute the total Born field u_B at any plane z_1 in an imaging system using the above transfer relation together with the parabolic approximation to Eq. (4.27). For plane wave illumination, the Rytov phase is obtained through the relation Eq. (5.7).

When the lens aperture is finite, the field in the *image plane* is simply that given by Eq. (8.16) convolved with the 2-D Fourier transform of the lens pupil function $\sigma_L(x_0, y_0)$ [GOODMAN (1968)]. In wavenumber space the angular spectrum of the field in the image plane is given by the well known expression

$$A_1(\alpha\kappa_x, \alpha\kappa_y; (1 - 1/\alpha)d_0) = \frac{1}{\alpha}\sigma_L(d_0\frac{\kappa_x}{k_0}, d_0\frac{\kappa_y}{k_0})\, A_0(\kappa_x, \kappa_y; 0) \tag{8.22}$$

so that, in the absence of aberrations, the lens pupil acts as an ideal low pass spatial filter. This fact was exploited in the imaging experiments of [YOUNG *et al.* (1984) and HOWARD *et al.* (1987)] who used image plane detector arrays sampling at the diffraction limited Nyquist frequency.

9 A NUMERICAL EXAMPLE

Imaging experiments are free of diffraction effects provided the Fresnel length for diffraction from the highest significant wavenumber features is much greater than the plasma dimension L. The problem of diffraction is more significant in the freely diffracting case, where the detecting plane may be somewhat remote from the plasma region. It is important to assess the degradation of the tomographically inverted phase information due to unaccounted diffraction effects.

The existence of significant ($\delta\varphi/\varphi \sim 10\%$) high K plasma density structures associated with MHD activity in the LT-4 tokamak has been reported by [NAZIKIAN (1989)]. As an example, we reproduce a set of experimental signatures obtained during strong MHD activity in LT-4 (Fig. 7). The line integrated signals vary strongly across the array (chordal separation 2 mm) with signicant energy for wavenumbers up to $K_p a \sim 40$ where $a \sim 10$ cm is the plasma radius. Nevertheless, for this imaging phase scintillation experiment, diffraction from such structures is completely negligible ($K_p z \lesssim .01$).

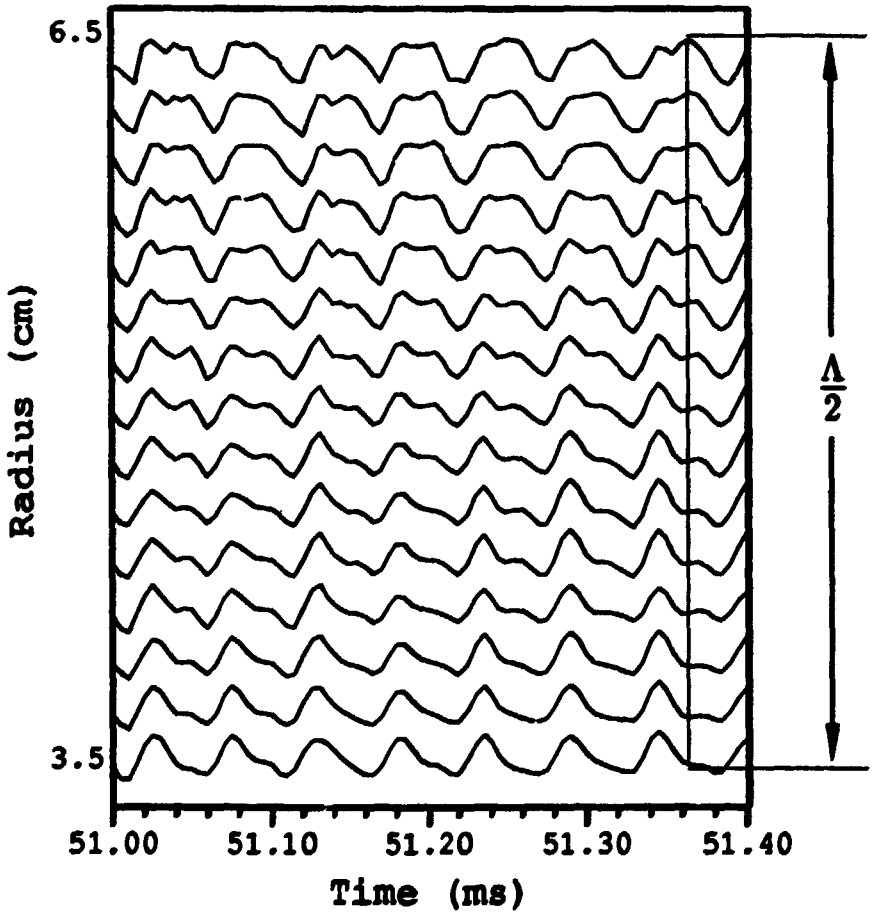

Figure 7: Interferometric signals produced by 15 adjacent scintillation channels during MHD activity on LT-4. Note the strong variation between chords.

For reasons of greater sensitivity and vibration noise immunity, far-infrared wavelengths are typically employed for standard interferometric measurements of the plasma density [PEEBLES *et al.* (1987)]. The effects of diffraction for these longer wavelength probes can be simulated

by computing the plane wave Rytov phase (Eq. (5.5)) for a synthetic density profile of similar bandwidth. The significance of diffraction for standard tomographic inversion of the calculated phase shifts can then be assessed. The assumption of plane wave illumination is a satisfactory approximation to experiments provided the plasma region lies near to the expanded Gaussian beam waist and the observer is in the Gaussian near field.

We consider a plasma distribution $n_e(x,z)$ that does not vary in the y direction, is bounded by the unit circle (radius $a = L/2 = 1$) with origin at the centre and is illuminated by the incident plane wave $\mathbf{k}_0 = (0,0,k_0)$. For the purposes of tomographic inversion we assume that only phase perturbations on the beam are measured. In preference to a particular model of the plasma distribution, we choose to examine diffraction from a weakly scattering, approximate point source centred in the plasma volume which is effectively bandlimited to some maximum wavenumber K_{max}. For this purpose it is convenient to use a truncated series approximation to the function $\delta(r)/r$ in terms of an orthogonal Zernike basis set (orthogonal radial polynomials and complex angular exponentials). Since the object is circularly symmetric, only $l = 0$ terms are required and we write

$$n_e(r) = \sum_{s=0}^{S} q_s R_s(r) \tag{9.1}$$

where $q_s = R_s(0)$ are real coefficients and $R_s(r)$ are zero order ($l = 0$) Zernike polynomials. This representation has the virtue of enabling computation of both the geometric projections and spectrum $\hat{N}(K)$ in terms of the object expansion coefficients q_s and analytic basis functions which are orthogonal in the projection and reciprocal spaces (Chebyshev and Neumann series respectively) (HOWARD, 1988). The distribution is effectively bandlimited to a maximum spatial frequency $K_{max} \sim 2S$ where S is the number of terms in the series expansion. Experimental interferometry systems typically yield no more than ~ 20 distinct channels in a given view of the plasma so that a maximum of ~ 20 Fourier coefficients describing the source $n = n_e/n_{cr}$ can be extracted from noise free data. With $\hat{N}$ effectively bandlimited to $K_{max} \sim 2S$, S channels evenly distributed in the interval $[0,1]$ will recover n_e to a bandwidth $K \sim \pi S$ without aliasing contamination. The chosen test distribution ($S = 20$, $K_{max} \sim 40$) and its spectrum are illustrated in Fig. 8.

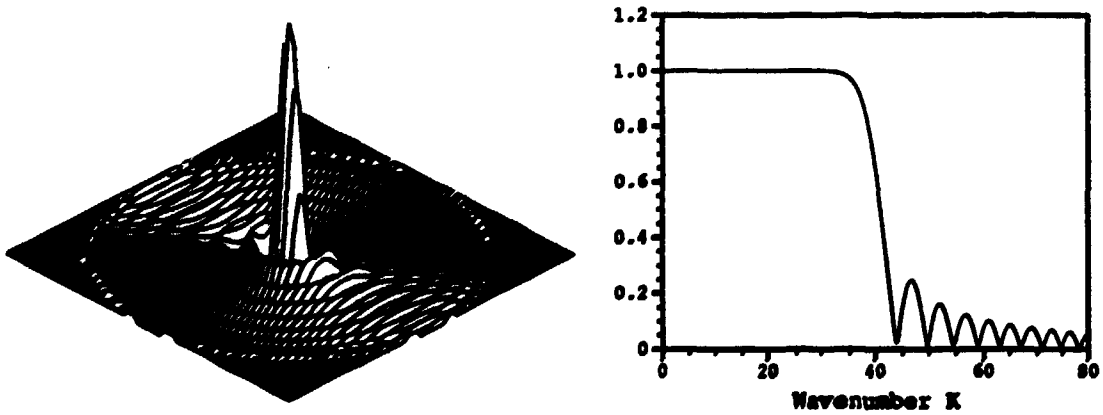

Figure 8: Circularly symmetric test distribution ($S = 20$) and the modulus of its Fourier transform. This object is effectively bandlimited to $K_{max} \sim 2S$.

With the above mentioned frequency plane representation, we have computed the transform of the plane wave Rytov phase Ψ_p and in Fig. 9 present grey scale contour plots of the spatial evolution of the real and imaginary parts of ψ_p. The distance scales are in units of plasma radius and the diffraction patterns have been calculated for an incident wavelength $\lambda = .002$ ($K/k_0 \sim .01$) to a distance $z = 10$ from the plasma midplane. For a Gaussian beam waist $w_0 = 1$ the plane wave approximation to the Gaussian phase φ_G is reasonably well satisfied ($K_P K_G z^2 \sim 0.3$, $z = 10$). A plasma of radius ~ 20 cm corresponds to a probing wavelength $\lambda \sim 400$ μm and the plotted diffraction patterns extend to 2 m from the plasma. The critical density $n_{cr} \approx 7 \times 10^{21}$ m^{-3} ensures that the weak fluctuation approximation $n_e/n_{cr} \ll 1$ for the Rytov phase is well satisfied for typical tokamak electron densities. Under these conditions, diffraction effects are apparent even at the edge of the plasma ($z = 1$). Amplitude perturbations are noticeable and the phase profile has departed somewhat from a purely geometric projection.

This deterioration is revealed in the quality of the geometric Abel inversions of the diffracted phase profile as a function of the dimensionless parameter $K_P z$. Specifically, we present (Fig. 10) geometric Abel inversions of the phase component of the field at the set of fixed distances $z = 1,(1),6$ ($K_P z = 0.25,(0.25),1.5$). The Abel inversions are obtained by computing the zero-order Hankel transform of the anti-Hermitian part of Ψ_p. Implicit is the assumption that the values of Ψ_p lie along a straight cut through the origin of the transform plane. The reconstructed peak of the impulse source attains the input value to within 10% only for $K_P z \lesssim 0.25$. With this as a measure of tolerable degradation, the satisfactorily transmitted bandwidth reduces as $z^{1/2}$ without the use of imaging techniques. However, not only is the transmitted bandwidth compromised by diffraction, the wave fields diffracted from structures having wavenumbers in excess of this diffraction limit will spoil the integrity of any reconstruction based purely on geometric inversion procedures. In such cases, it is imperative that diffraction effects be considered and that tomographic inversions be obtained using a Fourier plane interpolation technique similar to that suggested by [KAK (1985)]. It must be emphasised, however, that both real and imaginary parts of the complex Rytov phase must be determined to properly establish the object transform.

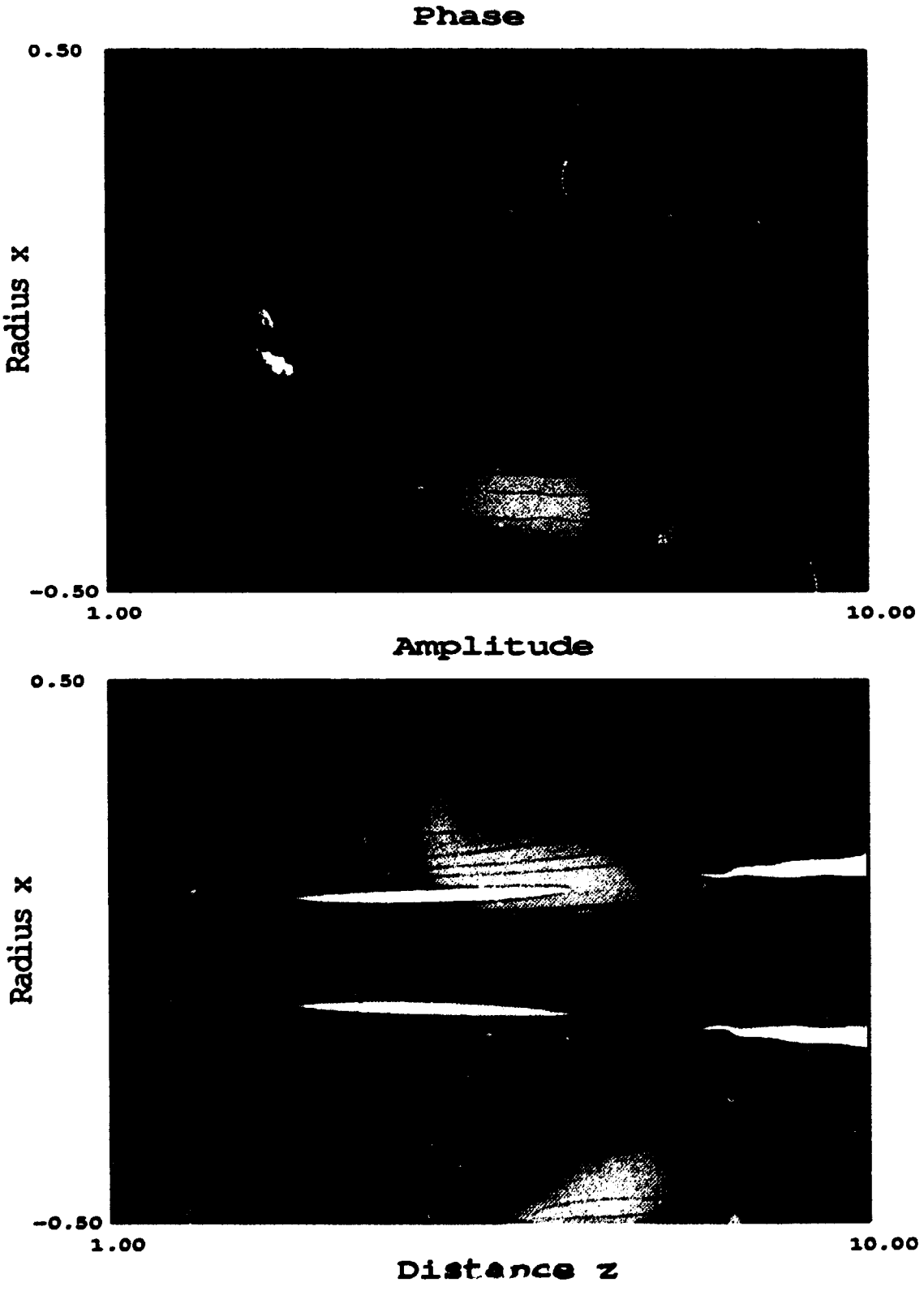

Figure 9: Grey scale contour plots showing the spatial evolution of the real (bottom) and imaginary (top) parts of the Rytov phase for a "bandlimited" point source ($S = 20$). The same contour levels are used for the display of both images.

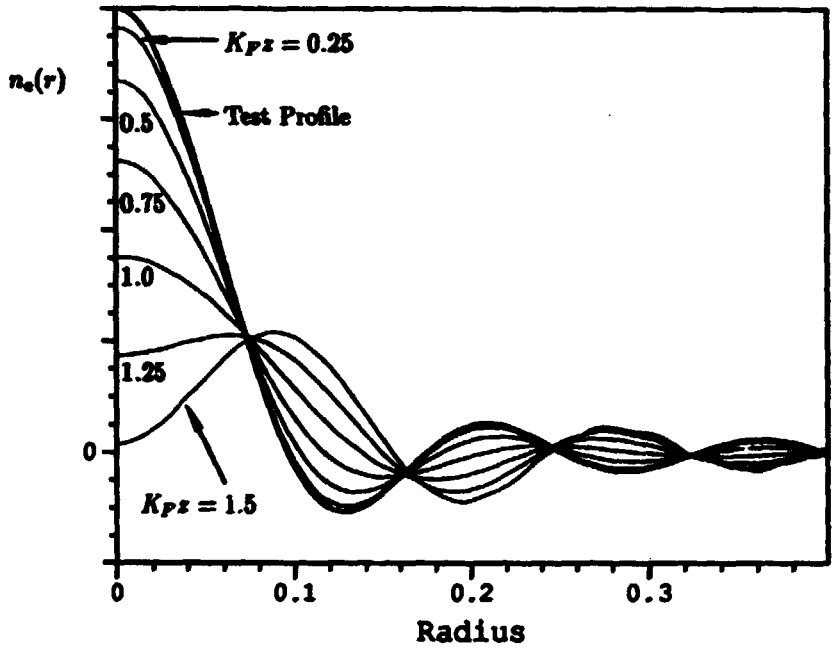

Figure 10: Abel inversions of φ_e at $z = 1,(1),6$ for the field diffracted from the source shown in Fig. 7 and for a probing wavelength $\lambda_0 = 0.002$. The corresponding values of the parameter $K_p z$ are marked on the graph. The bold curve is the test profile.

10 CONCLUSION

In this paper we have introduced a powerful and intuitive formalism for the analysis of near field imaging and scattering experiments on magnetically confined plasmas. New results for Gaussian beam diffraction in a plasma have also been established. These results will find extensive application to a range of scattering phenomena in both near and far fields in a following paper.

It is shown that only when certain quite stringent conditions are met do interferometric phase measurements accurately approximate geometric line integrals of the plasma density distribution. Numerical simulations of diffraction from an impulse source bandlimited to wavenumbers typical of those occurring in fusion plasmas have been performed. These computations confirm the need to account for diffraction during tomographic inversion of line of sight measurements.

REFERENCES

[] BANOS, A., *Dipole Radiation in the Presence of a Conducting Half Sphere* (Pergamon, Oxford, 1966).

[] BRACEWELL,R.N., *Image Reconstruction in Radio Astronomy* in "Image Reconstruction from Projections: Implementation and Applications" G.T. Herman, ed. (Springer-Verlag, Berlin, 1979) p81-104.

[] CLIFFORD, S.F., *The Classical Theory of Wave Propagation in a Turbulent Meium* in "Laser Beam Propagation in the Atmosphere",p10, Ed. J.W. Strohbehn (Springer-Verlag, New York, 1978).

[] GOODMAN, J.W., *Introduction to Fourier Optics*, (McGaw-Hill, San Francisco, 1968).

[] GOODMAN, J.W., *Statistical Optics*, (John Wiley and Sons, New York, 1985).

[] HOLZHAUER, E. and MASSIG, J.H., *An analysis of Optical Mixing in Plasma Scattering Experiments*, Plasma Physics, 20, 867-877 (1978)

[] HOWARD,J., DOYLE,E.J., REIBIZ,G., SAVAGE,R.L., PEEBLES,W.A., GULL,S.F., LUHMANN,N.C.,Jr., *Two Dimensional Imaging Interferometry on the Microtor Tokamak*, Proc. 14th European Conference on Controlled Fusion and Plasma Physics, (1987) 1310-1313

[] HOWARD, J., *Tomography and Reliable Information*, JOSA 5, 999 (1988).

[] HOWARD,J., *A Novel Scanning Interferometer for the H-1 Heliac* To be submitted to Rev. Sci. Instrum. (1989)

[] HUGENHOLTZ, C.A.J. and MEDDENS, B.J.H. *Multichannel CO_2-Laser Interferometer using a PbSnTe Detector Array*, Rev. Sci. Instrum. 53, 171-174 (1982)

[] ISHIMARU, A., *Fluctuations of a Beam Wave Propagating Through a Locally Homogeneous Medium* Radio Sci. 4 295-305 (1969 a)

[] JACKSON, J.D., *Classical Electrodynamics* (John Wiley and Sons, New York, 1975).

[] JACOBSON, A.R., *Interferometric Studies of Plasma Density Fluctuations Propagating Along the Major Radius in ZT-40M, Using Time-Delayed Correlation Techniques*, Plasma Physics, 24, 1111-1121 (1982)

[] JAMES, B.W. and YU, C.X., *Diffraction of Laser Radiation by a Plasma Wave - the Near and Far Field Limiting Cases*, Plasma Physics and Controlled Fusion, 27, 557 (1985)

[] KAK, A.C. *Tomographic Imaging with Diffracting and Non-Diffracting Sources*, in "Array Signal Processing" Ed. S. Haykin (Prentice-Hall Inc., New Jersey 1985).

[] KIM, S.K., BROWER, D.L., PEEBLES, W.A. and LUHMANN, N.C. Jr. *Experimental Measurement of Electron Particle Diffusion from Sawtooth-Induced Density-Pulse Propagation in TEXT*, Phys. Rev. Lett., 60, 577 (1988)

[] KLEIN, W.R. and COOK, W.D. *Unified Approach to Ultrasonic Light Diffraction*, IEEE Trans. on Sonics and Ultrasonics, SU-14 123-134 (1967)

[] LEE, R.W. and HARP, J.C. *Weak Scattering in Random Media, with Applications to Remote Probing* Proc. IEEE 57 375-406 (1969)

[] MUELLER, R.K., KAVEH, M. and IVERSON, R.D., *A New Approach to Acoustic Tomography Using Diffraction Techniques* Acoust. Imag., 8, 615-628 (1980)

[] NAZIKIAN, R. *Interferometric Study of Density Fluctuations in a Tokamak Plasma*, Thesis, A.N.U. (1989)

[] NAZIKIAN, R. and SHARP, L.E., CO_2 *Laser Scintillation Interferometer for the Measurement of Density Fluctuations in Plasma Confinement Devices*, Rev. Sci. Instrum., 58, 2086 (1987)

[] PEEBLES, W.A., SAVAGE, R.L., Jr., BROWER, D.L., KIM, S.K., LEHECKA, T., HOWARD, J., DOYLE, E.J., LUHMANN, N.C., Jr. *Plasma Diagnostic Applications on the TEXT Tokamak Using a High-Power Twin-Frequency Optically Pumped Far-Infrared Laser*, Int. J. Infrared and Millimeter Waves, 8 1355-63 (1987)

[] SHARP, L.E., *The Measurement of Large Scale Density Fluctuations in Toroidal Plasmas from the Phase Scintillations of a Probing Electromagnetic Wave*, Plasma Physics and Controlled Fusion, 25, 781 (1983)

[] SHEWELL, J.R. and WOLF, E. *Inverse Diffraction and a New Reciprocity Theorem*, J. Opt. Soc. Am., 58 1596-1603 (1968)

[] SIEGMAN, A.E., *An Introduction to Lasers and Masers*, (McGraw-Hill, New York, 1971).

[] SHEFFIELD, J., *Plasma Scattering of Electromagnetic Radiation* (Academic Press, New York, 1975).

[] SLANEY, M., KAK, A.C. and LARSEN, L.E. *Limitations of Imaging with First Order Diffraction Tomography*, IEEE Trans. Microwave Theory Tech., MTT-32, 860-873 (1984)

[] STROHBEHN, J.W., *Line-of-Sight Wave Propagation Through the Turbulent Atmosphere*, Proc. IEEE 56 1301-18 (1966)

[] SURKO, C.M. and SLUSHER, R.E. Physics Fluids, 23 2425 (1980)

[] TATARSKI, V.I., *Wave Propagation in a Turbulent Medium* (Dover, New York, 1967).

[] WEISEN, H., HOLLENSTEIN, CH. and BEHN, R. *Turbulent Density Fluctuations inthe TCA Tokamak*, Plasma Physics and Controlled Fusion, 30, 293-309 (1988)

[] WOLF, E., *The Three Dimensional Structure Determination of Semi-Transparent Objects from Holographic Data*, Opt. Commun., 1, 153 (1969)

[] YOUNG, P.E., NEIKIRK, D.P., TONG, P.P., RUTLEDGE, D.B. and LUHMANN, N.C.Jr. *Multichannel Far-infrared Phase Imaging for Fusion Plasmas*, Rev. Sci. Instrum. 56, 81-89 (1984)